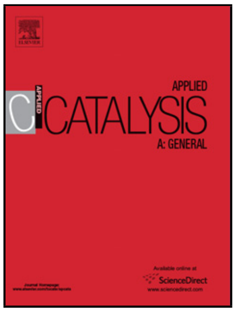

Title: Effect of Zn/Al ratio of Ni/ZnO-Al_2O_3 catalysts on the catalytic deoxygenation of oleic acid into alkane

Author: Lei Chen Feng Zhang Guangci Li Xuebing Li

PII: S0926-860X(16)30551-8
DOI: http://dx.doi.org/doi:10.1016/j.apcata.2016.11.012
Reference: APCATA 16060

To appear in: *Applied Catalysis A: General*

Received date: 22-7-2016
Revised date: 6-11-2016
Accepted date: 9-11-2016

Please cite this article as: Lei Chen, Feng Zhang, Guangci Li, Xuebing Li, Effect of Zn/Al ratio of Ni/ZnO-Al2O3 catalysts on the catalytic deoxygenation of oleic acid into alkane, Applied Catalysis A, General http://dx.doi.org/10.1016/j.apcata.2016.11.012

Graphical abstract

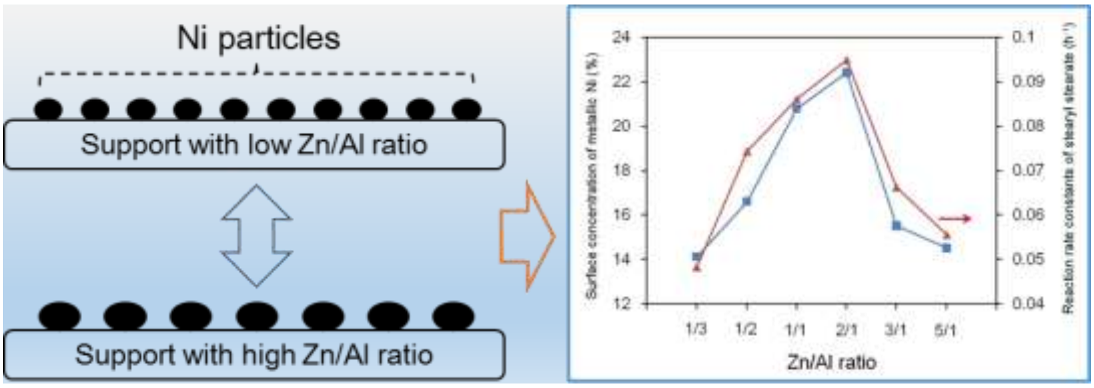

Research highlights

1. The addition of Zn atoms into support leads a decrease in metal-support interaction.

2. Weakening metal-support interaction favors the reduction of surface Ni species.

3. HDO activity of catalyst depends strongly on the proportion of exposed metallic Ni.

Effect of Zn/Al ratio of Ni/ZnO-Al_2O_3 catalysts on the catalytic deoxygenation of oleic acid into alkane

Lei Chen, Feng Zhang, Guangci Li,* Xuebing Li*

Key Laboratory of Biofuels, Qingdao Institute of Bioenergy and Bioprocess Technology, Chinese Academy of Sciences, Qingdao, 266101, PR China

Abstract: Ni-based catalysts supported on Zn-Al composite oxides have been prepared for the catalytic deoxygenation of oleic acid into diesel-ranged alkanes, and the effects of the Zn/Al ratio on the physico-chemical properties of the supports and the deoxygenation activity of the final catalyst were investigated in detail. The results showed that higher Zn/Al ratios led to lower specific surface area of the supports and weakening of the interaction between Ni species and supports thereby improving the reducibility of Ni species. However, higher Zn/Al ratios may limit the dispersion of Ni species, leading to a decrease in the exposure of metallic Ni. Because the conversion and deoxygenation of the reactants mainly depended on the hydrogenation capability of the catalysts which was controlled by the amount of exposed metallic Ni, the catalyst with a Zn/Al ratio of 2/1 showed the highest hydrogenation rate and alkane yield. Further decreasing the Zn/Al ratio led to strong metal-support interaction, making the Ni species difficult to reduce, which may also inhibit the formation of alkane products. In addition, the change in Zn/Al ratio affected intermediate type, which could affect the yield of alkane products.

Keywords: Biodiesel; Zn-Al composite oxide; Deoxygenation; Oleic acid; Alkane.

---

* Corresponding authors. Tel.: +860532080662759; Fax: +86 532 80662759. Email: ligc@qibebt.ac.cn (G. Li); lixb@qibebt.ac.cn (X. Li).

1. Introduction

The rapid increase in the consumption of transportation fuels and the environmental pollution has spurred the development of clean and sustainable fuels worldwide [1]. Among the renewable fuels, biodiesel has received significant attention in the past decade because it can be blended with petroleum-based diesel in all proportions and used directly without further modification [2]. Despite this, biodiesel suffers from high oxygen content, high pour point, poor thermal and chemical stabilities, and low energy density issues [3,4]. In order to overcome them, catalytic hydrodeoxygenation (HDO, removal of oxygen atoms) of biodiesel or vegetable oils for producing diesel-ranged hydrocarbon fuels has been intensively investigated in recent years [5-7].

Three different groups of catalysts have been widely used for HDO reactions: (i) supported sulphided transition metal catalysts [8-10]; (ii) supported noble metal catalysts [11-13]; and (iii) supported reduced transition metal catalysts [14-16]. The noble metal catalysts show high activity and stability, although their limited reserves and high cost inhibit their application on a large scale. Sulphided catalysts catalytically convert biodiesel into hydrocarbons and have been industrialized for many years, although their use requires the addition of sulfur-containing compounds such H_2S or CS_2 to maintain the catalytic activity [17]. However, these catalysts suffer from the generation of sulfur residues along with the reaction products and H_2S emissions, thereby increasing the operating cost. Having this in mind, supported reduced transition metal catalysts have been developed showing high liquid hydrocarbon yields during the conversion of vegetable oils. Solid acid materials such as SAPO-11 [18,19], Al-SBA-15 [20-22], Hβ [23,24], and HZSM-5 [25,26] are typically used as supports for these catalysts. Because of their strong acid strength, cracking and isomerization reactions are inevitable, thus affecting the composition and yield of the final liquid product. Moreover, these supports readily produce carbon deposition during the HDO process thereby reducing or even deactivating the catalytic activity. In view of this, weak acid (e.g., active Al_2O_3) and neutral (SiO_2) supports have been tested in the deoxygenation of fatty acids, although they showed poor fatty acid conversions [27].

Relative to the solid acid, solid bases have been significantly used as catalysts or supports in many fields of industrial chemical. In terms of catalytic deoxygenation, these materials have revealed some interesting properties. For instance, King and Olson found that the intramolecular carboxyl groups of 2-furoic acid and carbonates can be directly removed via decarboxylation catalyzed by hydrotalcite-like solid bases [28,29]. In addition, it is well known that the surface of solid bases possesses a large number of coordinatively unsaturated sites (so-called oxygen vacancies), which can activate oxygen atoms of fatty acid and thereby promote their removal [30,31]. Therefore, solid bases are considered potential catalyst supports for the HDO of vegetable oils and their derivatives, and their feasibility has been confirmed in our previous work [32] in which several supported Ni/MO-Al_2O_3 catalysts (M = Mg, Ca, Ni, Cu, and Zn) were prepared for the HDO of oleic acid. These results revealed that ZnO-Al_2O_3 composite is a promising support for highly efficient conversion of fatty acids into *n*-alkanes because of its moderate base strength. In this sense, several parameters including reaction time, reaction temperature, H_2 pressure, and Ni loading were investigated. According to the compositions of gas product, we found that the oxygen atoms in oleic acid were mainly removed in the form of carbon monoxide through a decarbonylation reaction. Furthermore, we carried out recycling experiments of a Ni/ZnO-Al_2O_3 catalyst and its catalytic activity toward the conversion of glycerol trioleate was determined.

The physico-chemical properties of ZnO-Al_2O_3 composite supports can be easily modified by changing the Zn/Al ratio, which remarkably affects the overall catalytic activity of these materials during HDO. Thus, this work focused on the effect of the Zn/Al ratio on the catalytic deoxygenation of fatty acids. As expected, the Zn/Al ratio played a key role in the catalytic deoxygenation activity, particularly in the hydrogenation activity of the catalysts. The addition of Zn atoms in moderate amounts can efficiently improve the dispersion of Ni species, increasing the effective contact area of metallic Ni and eventually resulting in high conversions of oleic acid and alkane yields. On the other hand, excessive addition of Zn atoms may lead to the formation of a single ZnO phase in large amounts, and this component can react with the fatty acid during the reaction to form zinc stearate decreasing the yield of alkane.

2. Experimental Section

2.1. Preparation of ZnO-Al_2O_3 supports

ZnO-Al_2O_3 supports were prepared through a hydrothermal synthesis process followed by thermal decomposition at high temperature. Typically, *m* mmol of

$Zn(NO_3)_2{\cdot}6H_2O$, *n* mmol of $Al(NO_3)_3{\cdot}9H_2O$, and a certain amount of $CO(NH_2)_2$ were dissolved into 40 mL of deionized water to form a colorless solution, where the sum of *m* and *n* was 6.0 and the molar ratio [urea]/[NO_3^-] was 3.0. The resulting solution was subsequently transferred into a 100 mL Teflon-lined stainless autoclave and heated at 180 °C for 3 h. After that, the obtained precipitate was collected by filtration, washed with deionized water until neutral pH, and then dried overnight in an oven at 80 °C. Finally, the dry substance was heated in air from room temperature to 500 °C at a rate of 2 °C/min and maintained for 4 h, leading to the formation of the $ZnO\text{-}Al_2O_3$ support.

To investigate the effect of the Zn/Al ratio on the catalytic HDO activity, several supports were prepared following the above procedure. Thus, the ratio was controlled to be 1/3, 1/2, 1/1, 2/1, 3/1, and 5/1, and the corresponding supports were labeled as Zn1Al3, Zn1Al2, Zn1Al1, Zn2Al1, Zn3Al1, and Zn5Al1, respectively.

2.2. Preparation of $Ni/ZnO\text{-}Al_2O_3$ catalysts

$Ni/ZnO\text{-}Al_2O_3$ catalysts were prepared by an incipient wetness impregnation method and the procedure was performed as follows: 3.4 mmol of $Ni(NO_3)_2{\cdot}6H_2O$ was dissolved in 2.7 mL of deionized water, and the solution was subsequently added dropwise to 1.8 g of the as-prepared $ZnO\text{-}Al_2O_3$ support while agitating at room temperature for 2 h. The obtained substance was then dried overnight at 80 °C and then calcined under flowing N_2 (flow rate: 80 ml min^{-1}) at 400 °C for 4 h, followed by a reduction at 500 °C under flowing of H_2 (flow rate: 80 ml min^{-1}) for 4 h. The heating rate for both the calcination and the reduction processes was 2 °C min^{-1}. The obtained sample was labeled as Ni/ZnO-Al_2O_3 catalyst with a 10 wt.% Ni content. The catalysts with different ZnO-Al_2O_3 supports were prepared and labeled as Ni/Zn1Al3, Ni/Zn1Al2, Ni/Zn1Al1, Ni/Zn2Al1, Ni/Zn3Al1, and Ni/Zn5Al1.

2.3. Characterization of the materials

The crystalline structures of the supports were characterized by X-ray diffraction (XRD) on a Bruker AXS-D8 advance powder diffractometer with a Cu Kα radiation source (wavelength: 1.5406 Å) operating at 40 kV and 40 mA. The samples were measured with a scanning rate of 4°/min and a diffraction angle (2θ) ranging from 5 to 80°.

The textural properties of the supports were measured by nitrogen adsorption-desorption isotherms at - 196 °C on a Quantachrome AutoSorb-6B adsorption analyzer. Prior to the measurements, each sample was degassed under vacuum at 140 °C for 6 h. The specific surface area was calculated using the Brunauer-Emmett-Teller (BET) method, and the pore volumes and pore sizes were determined by the Barrett-Joyner-Halenda (BJH) method from the desorption branch of the isotherms.

Elemental analysis of the prepared catalysts were performed using inductively coupled plasma optical emission spectroscopy (ICP-OES) on a Leeman Labs Prodigy spectrometer. The measured contents of nickel were compared to standard to determine actual concentrations.

The reduction of the Ni species on the supports was investigated by hydrogen temperature-programmed reduction (H_2-TPR) measurements on a Micromeritics

AutoChem II 2920 chemisorption analyzer. Approximately 100 mg of the sample was used for each measurement. Each sample was charged in a U-shaped quartz cell reactor and pretreated under flowing Ar (flow rate: 20 ml min^{-1}) at 300 °C for 1 h (ramp rate: 10 °C min^{-1}), and then cooled to 100 °C. Afterwards, a mixture of 10 vol.% H_2/Ar was introduced into the sample tube at a flow rate of 20 ml·min^{-1}. These conditions were maintained for 20 min, after which the sample was heated to 900 °C at a rate of 10 °C·min^{-1} and maintained at this temperature for 20 min, during which the hydrogen consumption was measured with a thermal conductivity detector (TCD) calibrated by reduction of fresh CuO.

The morphologies of the samples were observed on a Hitachi S-4800 field emission scanning electron microscopy (FE-SEM) device with an accelerating voltage of 1.5 kV. Transmission electron microscopy (TEM) analyses was carried out on a JEM-2100HR electron microscope with an accelerating voltage of 200 kV. The reduced catalysts were ultrasonically dispersed in ethanol and dropped onto a carbon-coated copper grid. At least 200 Ni particles were observed in order to determine the Ni nanoparticle size distribution.

The active metal existing forms of the catalysts were analyzed by X-ray photoelectron spectroscopy (XPS) on an Escalab 250Xi Thermo Spectrometer equipped with a monochromatic X-ray source of Al Kα under ultra-high vacuum (2-3 × 10^{-6} Pa) and a hemispherical analyzer. The XPS data from the regions related to the C 1s, O 1s, and Ni 2p core levels were recorded for each sample. The obtained spectra were fitted by mixed Gaussian-Lorentzian functions. The binding energies (BE) were internally calibrated by the reference deposit C 1s binding energy (BE).

2.4. Activity tests and product analyses

The catalytic deoxygenation of oleic acid was carried out in a 100 mL batch stainless autoclave furnished with a mechanical stirrer. In a typical reaction, 0.2 g of fresh catalyst, 2.0 g of oleic acid, and 30.0 g of decalin were loaded in the autoclave. Prior to the reaction, the reactor was purged three times with H_2 to remove the inside air and then pressurized to 2.5 MPa at ambient temperature. The reaction system was subsequently heated to 280 °C and maintained at this temperature for 360 min at a stirring rate of 600 rpm. Finally, the reaction system was cooled to ambient temperature, and the liquid products were collected for subsequent analysis.

The products in the gas phase were analyzed by gas chromatography mass spectrometry (GC-MS) with a TCD and a HP-PLOT/Q column (30 m, 0.32 mm inner diameter, 20 μm film thickness). The liquid products were analyzed by GC-MS with a flame ionization detector (FID) and a HP-INNOWAX column (30 m, 0.25 mm inner diameter, 0.25 μm film thickness). *N*-octadecane was used as an external standard for the quantification of the liquid products. Besides, Fourier transform infrared spectroscopy (FT-IR) spectra were recorded using a Nicolet 6700 spectrometer to identify the -C(O)O- group in the liquid products. Considering that zinc stearate as a by-product cannot be dissolved into decalin and analyzed by GC-MS, the amount of zinc stearate was obtained by a gravimetric method. The generated zinc stearate can be obtained by heating, centrifugation, washing, and drying processes.

3. Results and Discussion

3.1. Crystalline structures of the supports

Figure 1 shows the diffraction patterns of the Zn-Al composite precursors with different Zn/Al ratios. As observed, the crystalline structures markedly changed as the Zn/Al ratio increased. Specifically, in the case of the precursor with a Zn/Al ratio of 1/3 (Figure 1a), most of the diffraction peaks were assigned to the boehmite (AlOOH) phase (JCPDS #21-1307), while only a very weak peak attributed to the $Zn(OH)_2$ phase (JCPDS #24-1444) was observed, indicating that Zn atoms were well dispersed into the boehmite phase. Increasing the Zn/Al ratio to 1/2 (Figure 1b) did not change the crystalline structure of the precursor except for some slight differences in the intensity of the diffraction peaks. At a Zn/Al ratio of 1/1 (Figure 1c), the diffraction peaks of the boehmite phase nearly disappeared, and other diffraction peaks assigned to the $ZnAl_2O_4$ phase (JCPDS #05-0669) appeared instead. These results suggest that most of the Al atoms were bonded with Zn atoms through oxygen-bridged bonds to directly form Zn-Al composite oxides under hydrothermal conditions. Meanwhile, the excess Zn atoms unbonded to Al were spontaneously transformed to $Zn_4(CO_3)(OH)_6$ (JCPDS #11-0287) owing to the coexistence of CO_3^{2-} and OH^- anions in the system. This result reveals that a Zn/Al ratio of *ca.* 1/1 is a boundary value for the formation of well-dispersed Zn-Al composites with low crystallite size. When the Zn/Al ratio exceeds this value, the excess Zn atoms nucleate, grow, and aggregate to form a single Zn-containing phase such as $Zn(OH)_2$ and $Zn_4(CO_3)(OH)_6$ owing to the lack of Al atoms, with this process being more pronounced with the amount of Zn atoms added. Therefore, a further increase of the Zn/Al ratio led to higher diffraction intensities without affecting the phase composition (Figures 1d-f).

Figure 2 shows the diffraction patterns of the samples obtained by heating the above precursors at 500 °C for 4 h. After the heat treatment, all precursors were transformed into ZnO-Al_2O_3 composite oxides, and their crystalline structures varied with the Zn/Al ratio. For instance, when the Zn/Al ratio was lower or equal to 1/1, the samples mainly consisted of $ZnAl_2O_4$ and γ-Al_2O_3 phases (JCPDS #49-0134) (Figures 2a-c), with the latter phase undoubtedly originating from a boehmite phase transformation via dehydration at high temperature. It is worth noting that diffraction peaks corresponding to Zn-Al hydrotalcite-like compounds were not found in the XRD patterns of their precursors, revealing that the $ZnAl_2O_4$ phase was not formed upon thermal decomposition of hydrotalcite-like compounds. Considering the compositions of these precursors, it is thought that a minor amount of the amorphous $ZnAl_2O_4$ phase was generated during the precursor formation, and most of this phase likely arose from a solid phase reaction between $Zn(OH)_2$ and boehmite during the heat treatment of the precursors. The intensity of the diffraction peaks assigned to the $ZnAl_2O_4$ phase gradually increased with the Zn/Al ratio. When this ratio was higher than 1/1, diffraction peaks corresponding to a ZnO phase (JCPDS #65-3411) were identified and became more evident with a further increase in the Zn/Al ratio (Figures 2d-f). During this process, the amount of the $ZnAl_2O_4$ phase decreased accordingly with the decrease of the Al content. Finally, the $ZnAl_2O_4$ phase was found to be highly dispersed on ZnO, as its diffraction peaks were gradually covered by those of ZnO and finally disappeared. The obtained supports mainly consisted of ZnO and $ZnAl_2O_4$

phases, with the ZnO phase being formed by $Zn(OH)_2$ dehydration and $Zn_4(CO_3)(OH)_6$ decomposition.

3.2. Morphologies of the supports

Based on above XRD characterizations, the composition of the supports was found to be closely dependent on the Zn/Al ratio. As the ratio was increased, the composition changed from $ZnAl_2O_4$-Al_2O_3 to ZnO-$ZnAl_2O_4$ mixed oxide, and this change should affect the morphology and microstructure of the supports. In view of this, all supports were characterized by SEM (Figure 3). The support having lower Zn content was found to be mainly constructed of small and unshaped particles in mixture with a minor amounts of sheet-like structures (Figure 3a). An increase in the Zn/Al ratio gradually increased the amount and the size of sheet-like structures (Figures 3b and c). At Zn/Al ratios exceeding 1/1, these sheet-like structures markedly changed both in size and shape (they became wider and thicker and their shape more uniform). This change was highly consistent with the XRD characterization of the precursors showing noticeable changes in the diffraction patterns and peak intensities upon increasing the Zn/Al ratio from 1/1 to 2/1. Further increase of the Zn/Al ratio changed the shape of these micro-sheets toward more regular, and the surface of these particles became smoother (Figures 3e and f). As shown by with the patterns in Figure 2, the crystallites of $ZnAl_2O_4$ aggregated into larger irregular particles, while those of ZnO preferentially grew into regular micro-sheets. These differences will affect the textural properties (i.e., specific surface area, SSA, and pore volume, PV) of the supports.

3.3. Textural properties of the supports

The textural properties of the supports were measured by a N_2-adsorption method, and the corresponding adsorption-desorption isotherms are displayed in Figure S1 in the Supporting Information. All the isotherms showed hysteresis loops at relative pressure above 0.4 and no distinct uptake at lower relative pressures, suggesting the absence of micropores in these supports. The isotherms were of type IV for all the supports except for Zn1Al3, which showed an isotherm type II. The isotherm shape was form to shift from type II to type IV with the Zn/Al ratio. This evolution indicates that the as-prepared supports are mesoporous materials, and their pore size decreased with the Zn/Al ratio, as verified with the decreasing hysteresis loop areas. Additionally, the hysteresis loops for all supports were of type H3, implying that the pores mainly arose from the gaps between aggregates or agglomerates of particles (e.g., plates or edged particles like cubes) [33]. This result was in agreement with the SEM observations suggesting that the pores were formed via stacking of sheet-like structures.

The pore structure parameters of the supports (SSA and PV) are listed in Table S1. The SSA decreased with the Zn/Al ratio. The isotherms revealed that the pores were made by the stacking of the secondary particles formed by the aggregation of the primary crystallites. Thus, the particles with lower size may generate additional pores providing higher SSA values, while the supports composed of larger secondary particles such as Zn5Al1would present lower SSA. The SSA of the supports markedly decreased with the Zn/Al ratio increasing from 1/1 to 2/1, in good agreement with the observed changes in morphology and particle size. Since a further increase of the Zn content did not change the size of the micro-sheets noticeably, the SSA of the supports remained unchanged. In addition to the SSA, changes in the particle size affected the PV of the supports. Thus, for a certain amount of solid powder, larger particles would occupy more inner space, leading to lower PV. Both SSA and PV of the supports decreased to various degrees after Ni loading, whereas the SSA remained unchanged with the Zn/Al ratio (see Table 1).

3.4. Dispersion state and existing form of surface Ni species

The addition of Zn remarkable affected the SSA and the surface basicity of the supports, leading to different dispersion states of Ni species onto these supports. As seen from Figure 4, the average particle diameter of Ni species gradually increased from 2.7 to 29.7 nm with the Zn/Al ratio, suggesting that the addition of Zn was unfavorable for dispersion of Ni species. This phenomenon was induced by the following two factors. First, larger Zn contents decreased the SSA of the supports, and it is accepted that low SSA is unfavorable for the dispersion of active metals. Second, Ni species preferably interacted with the acidic alumina support to form Ni-O-Al bonds, with this interaction potentially inhibiting the migration and aggregation of Ni species and eventually improving its dispersion. In our case, the addition of Zn decreased the amount of acid sites and weakened the metal-support interaction, decreasing the Ni dispersion. Remarkably, Zn2Al1, Zn3Al1, and Zn5Al1 had nearly equal SSA values, although the Ni particle size on these supports increased with the Zn/Al ratio. These results indicate that the amount of surface base sites more critically determine the dispersion of the Ni species as compared to the SSA of the support.

In order to further investigate the underlying differences on the interaction of the Ni species with the support, H_2-TPR experiments were performed on the unreduced Ni-based catalysts while varying the Zn/Al ratios (Figure 5). The first reduction peak at *ca.* 260 °C was attributed to a weakly interacting NiO phase, while the second peak at 330-350 °C was ascribed to the reduction of a strongly interacting NiO phase. Furthermore, the additional peak over 500 °C can be assigned to a Ni-aluminate phase which is difficult to reduce [34]. This aluminate was likely formed via interaction of the Ni species with surface Al-OH groups of the supports. The reduction peak shifted toward lower temperatures with the Zn/Al ratio, indicating that the reduction of surface Ni species became easier. This tendency confirms that the interaction between the Ni species and the support was weakened upon Zn addition, which is in agreement with the results of the dispersion state of Ni species. According to the area of the reduction peak, the overall H_2 consumption per mass for each sample up to 500 °C was calculated to be 0.07, 0.16, 0.42, 0.43, 0.47, and 0.47 mmol g^{-1} for Ni/Zn1Al3, Ni/Zn1Al2, Ni/Zn1Al1, Ni/Zn2Al1, Ni/Zn3Al1, and Ni/Zn5Al1, respectively. These results further corroborate that the addition of Zn atoms weakened the interaction of Ni species with support, leading to easier reduction of these species. Complete Ni reduction to metallic Ni would result in a H_2 consumption of 1.7 mmol g^{-1}. Since this theoretical value is higher than those obtained experimentally, it can be induced that only a minor fraction of the Ni species were reduced to metallic Ni under the reduction conditions used herein.

XRD measurements were performed on the reduced Ni-based catalysts while varying the Zn/Al ratios to preliminarily investigate the composition of the surface Ni species (Figure 6). The standard pattern of metallic Ni (JCPDS #04-0850) presents two characteristic diffraction peaks at $2\theta = 44.6$ and 52.1°, which are assigned to Ni (111) and Ni (200), respectively. However, the peak corresponding to Ni (200) was not observed herein. The peak corresponding to Ni (111) (nearby $2\theta = 44.5°$) was partially covered by that of $ZnAl_2O_4$ (400) ($2\theta = 44.8°$) considering the close positions of both peaks and the higher amount of the $ZnAl_2O_4$ phase as compared to metallic Ni. The color of the unreduced catalysts shifted from yellow-green to black after the reduction, which indicates that metallic Ni was indeed generated. Based on these analyses, it is believed that the generated metallic Ni was well dispersed on the surface of the support, making it difficult to detect by XRD because of its very low size.

Those catalysts having Zn/Al ratios lower than 1/1 showed diffraction patterns similar to those of the corresponding supports. However, the characteristic peaks of the NiO phase at $2\theta = 43.3$ and 62.8° (JCPDS #44-1159) appeared for Zn/Al ratios higher than 1/1 (Figures 6d-f). These results also suggested that increasing the Zn/Al ratio is unfavorable for the dispersion of Ni species, with the black particles appearing in the TEM images being likely composed of unreduced NiO and metallic Ni rather than pure metallic Ni. As expected from the H_2-TPR experiments, only the surface layers of NiO crystallites were reduced, and thus the diffraction peaks corresponding to metallic Ni were not observed in the XRD patterns. By means of the Scherrer equation, the NiO crystallite size was calculated to be *ca.* 6-8 nm, which is significantly lower than the particle size calculated by TEM. These results indicated that these large particles are aggregates of several partially reduced NiO crystallites.

To further ascertain the existing form of the surface Ni species, XPS was employed on all the reduced Ni-based catalysts (Figure 7a). The Ni $2p_{3/2}$ band was deconvoluted in all cases into three peaks at binding energies of 851-860 eV, in which the peak at 851.8-853.4 eV was attributed to metallic Ni, while the other two peaks were assigned to NiO species (i.e., pure NiO at 854.1-855.5 eV and Ni aluminate at 855.6-856.7 eV [35-37]). The integral areas of the three peaks revealed the presence of large amounts of Ni aluminate on the surface of the catalysts, although this phase was not detected by XRD (Figure 7), probably because of its high dispersion. The binding energies of the three peaks decreased in different degrees with the Zn/Al ratio, indicating that the interaction of Ni species with the supports gradually decrease with this parameter, in agreement with the H_2-TPR results. The surface concentrations of metallic Ni (calculated with the relative area of its characteristic peak, Figure 7b), increased with the Zn/Al ratio reaching a maximum at Zn/Al = 2/1 and decreasing thereafter. This trend was not in agreement with the H_2-TPR calculations revealing larger amounts of metallic Ni with the Zn/Al ratio. Considering that XPS only detects the near-surface of the materials (i.e., testing depth is generally lower than 10 nm which is lower than the particle size of the Ni species for Ni/Zn3Al1 and Ni/Zn5Al1), only a fraction of the metallic Ni was detected. These results also indicate that a relatively large particle size was unfavorable for the exposure of internal metallic Ni atoms, thus affecting the hydrogenation ability of the catalysts.

3.5. Catalytic deoxygenation of oleic acid

In order to investigate the effect of the Zn/Al ratio on the overall catalytic activity, oleic acid diluted with decalin was selected as a reactant to test the catalytic deoxygenation behavior of the as-prepared Ni-based catalysts, and the liquid products were qualitatively analyzed with FT-IR spectroscopy (Figure 8). Most of the absorption peaks were attributed to the solvent except for those at v = 1712 and 1741 cm^{-1}, which were assigned to the stretching vibration of the C=O bonds of the fatty acid and the ester, respectively. In the case of the reactant, only the peak corresponding to the carbonyl group in the fatty acid was observed in the FT-IR spectrum. After the reaction with H_2, this peak became smaller and finally disappeared with the Zn/Al ratio, indicating that the addition of Zn favored the conversion of the fatty acid. An ester product was first generated (at the expense of the fatty acid) and then converted completely. In addition, some white substances were found on the surface of the used catalysts with Zn/Al ratios of 2/1, 3/1, and 5/1, and this substance was identified by FT-IR as zinc stearate (Figure S2). Other possible products such as alkanes, alcohols, and aldehydes were not clearly identified from the FT-IR spectra.

All the liquid products were quantitatively analyzed in detail to determine their compositions and distributions by GC-MS, and the results are summarized in Table 2. Because the double bonds in oleic acid can be easily saturated under the present reaction conditions, high conversions (higher than 99 %) were obtained for all the catalysts under study, although oxygen were not removed completely. In all the cases, the liquid products were mainly composed of five components (i.e., alkane, 1-octadecanol, stearic acid, stearyl stearate, and zinc stearate) and, as expected, their relative contents were closely dependent on the Zn/Al ratio of the support. A potential product such as octadecanal was not detected, which may be attributed to its low thermal stability and high reactivity. With respect to the gas phase (not shown), CO was the main product (versus CO_2 and CH_4) and its amounts was dependent on the amounts of C_{17} alkane. The generated CH_4 was thought to be derived from the reaction of CO or CO_2 with H_2 [25].

With regard to the target products, the alkane content (C_{17} + C_{18}) first increased and reached a maximum at Zn/Al = 2/1. Although this content then decreased to some extent, it was still higher than that obtained from the catalyst with a Zn/Al ratio of 1/3, indicating that the addition of Zn can promote the catalytic deoxygenation of oleic acid with an optimum Zn/Al ratio of 2/1. The amount of C_{17}-alkane in the target product was higher than 0.9 for all the catalysts, indicating that the alkanes were mainly produced via hydrodecarbonylation. Since the as-prepared catalysts were weak acids that cannot catalyze alkane cracking/isomerization reactions (as zeolite-type catalysts do), C_{17}- and C_{18}-alkane isomers or their cracking products were not found among the products. To further optimize the Zn/Al ratio, the other two catalysts (Zn/Al ratios of 1.5/1 and 2.5/1) were prepared and tested under the same reaction conditions (Table S1). Both of them showed lower alkane yields than Ni/Zn2Al1, confirming that 2/1 is the optimum Zn/Al.

Stearyl stearate, formed by esterification between 1-octadecanol and stearic acid intermediates, was the main by-product at Zn/Al ratios lower than 1/1. Our previous work confirmed that stearyl stearate was a very important intermediate, with most of the alkane product being produced through its subsequent conversion (rather than through the direct deoxygenation of fatty acids). Thus, the alkane yield was proportional to the stearyl stearate conversion [32]. Because the conversion of stearyl stearate to alkane involves a hydrogenolysis process, the catalysts are expected to have a high hydrogenation activity. According to the H_2-TPR results, the addition of Zn weakened the interaction between the Ni species and the support facilitating the formation of metallic Ni. Those catalysts having larger amounts of metallic Ni will have superior hydrogenation activity. Therefore, stearyl stearate was not detected and the content of alkane increased remarkably when the Zn/Al ratio was higher than 1/1. In spite of this, the content of Zn should be kept to a lower level since, according to XRD results, excess Zn atoms (uncoordinated with Al) are present in the final catalyst in the form of separated ZnO phase that will readily react with the fatty acid to form zinc stearate. Thus, the content of zinc stearate was found to be proportional to the Zn/Al ratio.

3.6. Hydrodeoxygenation of stearyl stearate

The above reaction data show that the stearyl stearate residue in the products markedly decreased with the Zn/Al ratio, which seems to indicate that increasing the Zn/Al ratio could effectively enhance the hydrogenation activity of the catalysts and the alkane yield. However, since the production of zinc stearate (favored by high

Zn/Al ratios) may change the final product distribution, this might affect the role of Zn in the hydrogenation reaction. Thus, stearyl stearate was selected as a starting material to investigate the effect of Zn on the final catalytic activity (Figure 9). The conversion of stearyl stearate over the different catalysts decreased in the following order Ni/Zn2Al1 > Ni/Zn1Al1 > Ni/Zn1Al2 > Ni/Zn3Al1 > Ni/Zn5Al1 > Ni/Zn1Al3, this trend being closely related to their hydrogenation activity as the conversion of stearyl stearate only depends on this parameter. This tendency was not in agreement with the results in Table 2 showing higher hydrogenation activities for Ni/Zn3Al1 and Ni/Zn5Al1 as compared to Ni/Zn1Al1 and Ni/Zn1Al2. This discrepancy is thought to be related to the formation of zinc stearate. Considering that zinc stearate was directly produced by the reaction between the fatty acid and the ZnO on the catalyst surface, while stearyl stearate was produced via esterification of the fatty acid with the 1-octadecanol produced by fatty acid hydrogenation. Thus, zinc stearate was formed prior to the stearyl stearate appearance. In the case of Ni/Zn3Al1 and Ni/Zn5/Al1, due to the formation of zinc stearate, a large amount of fatty acid was consumed thereby reducing the yield of stearyl stearate. Because zinc stearate was found to have a higher reactivity relative to stearyl stearate, the moderate hydrogenation activities of these two catalysts were enough to convert this intermediate, and thus stearyl stearate was not detected and most zinc stearate was transformed into alkanes.

All the above liquid products from stearyl stearate were also analyzed by GC-MS, and their compositions are listed in Table 3. Because the fatty acid cannot be obtained from stearyl stearate, stearic acid and zinc stearate were not present in these products.

In this case, octadecanal was determined to be the main by-product, and 1-octadecanol was only detected in a trace amounts (< 0.5 wt.%). The hydrogenolysis of stearyl stearate can be well described by a pseudo-first order kinetics equation, with the rate constants being closely related to the concentration of surface metallic Ni in the catalysts. As expected, increasing the Zn/Al ratio did not promote the hydrogenolysis of stearyl stearate. Instead, excess Zn negatively affected this reaction, even though higher Zn/Al ratios could lead to the formation of more metallic Ni. When considering the TEM, H_2-TPR, and XPS data, it was found that not only the amount but also the particle size of surface metallic Ni affected the hydrogenation rate of the catalysts. Weak metal-support interaction was confirmed to promote the reduction of surface Ni species, resulting in more metallic Ni exposed on the catalyst surface, more hydrogenation active sites and thus higher hydrogenation rates. However, weaken interactions lead to the migration and aggregation of Ni species (i.e., increase of the particle size) which would be located in the bulk of these particles. This would reduce the effective contact area of metallic Ni atoms with stearyl stearate, eventually limiting the catalytic activity. Thus, Ni/Zn1Al1 and Ni/Zn1Al2 showed higher alkane yields compared with Ni/Zn3Al1 and Ni/Zn5Al, although the former catalysts contained a lower amount of metallic Ni. In the case of Ni/Zn1Al1 and Ni/Zn2Al1, they showed nearly similar alkane yields depending on the concentration of exposed metallic Ni. However, considering that during the HDO of vegetable oils to alkanes large amounts of intermediate fatty acid will be produced, Ni/Zn2Al1 is thought to be more suitable for this process.

In addition, the content of octadecanal increased with the Zn/Al ratio, indicating that the addition of Zn inhibited the conversion of octadecanal. This may be also related to the overall hydrogenation activity, although the specific effect of Zn cannot be determined at present and need to be further investigated because of the different conversions of stearyl stearate obtained.

4. Conclusion

The investigation of the effect of the Zn/Al ratio on the catalytic deoxygenation of oleic acid showed that the addition of Zn led to the reduction of the SSA of the supports while also weakening the metal-support interaction and decreasing the dispersion of Ni species. This low dispersion promoted the migration and aggregation of Ni species into large particles thereby limiting the exposure of metallic Ni atoms. The concentration of surface accessible metallic Ni atoms and the final catalytic activity (particularly hydrogenation) of the catalysts decreased with the Zn/Al ratio. At a Zn/Al ratio of 2/1, the particle size of Ni species and the exposure degree of metallic Ni atoms reached a balance, resulting in optimum deoxygenation activity and maximum alkane yield (95.8 wt.%). Relatively low Zn/Al ratios may lead to strong metal-support interaction, which makes the Ni species difficult to reduce to metallic Ni and inhibits the conversion of oxygen-containing reactants.

Acknowledgement

Financial supports from the National Natural Science Foundation of China (No. 21506239; No. 21276263) are gratefully acknowledged. We also thank Dr. Y.P. Li (College of Chemical Engineering, China University of Petroleum, Qingdao, P.R.

China) for TEM analysis.

References

[1] H. Shi, J. Chen, Y. Yang, S. Tian, Fuel Process. Technol. 118 (2014) 161-170.

[2] A.K. Agarwal, Prog. Energy Combust. Sci. 33 (2007) 233-271.

[3] A.V. Bridgwater, G.V.C. Peacocke, Renew. Sust. Energy Rev. 4 (2000) 1-73.

[4] L.C. Meher, D.V. Sagar, S.N. Naik, Renew. Sust. Energy Rev. 10 (2006) 248-268.

[5] M. Mohammad, T.K. Hari, Z. Yaakob, Y.C. Sharma, K. Sopian, Renew. Sust. Energy Rev. 22 (2013) 121-132.

[6] P.M. Mortensen, J.-D. Grunwaldt, P.A. Jensen, K.G. Knuden, A.D. Jensen, Appl. Catal. A: Gen. 407 (2011) 1-19.

[7] J.K. Satyarthi, T. Chiranjeevi, D.T. Gokak, P.S. Viswanathan, Catal. Sci. Technol. 3 (2013) 70-80

[8] G.W. Huber, P. O'Connor, A. Corma, Appl. Catal. A: Gen. 329 (2007) 120-129.

[9] D. Kubička, L. Kaluža, Appl. Catal. A: Gen. 372 (2010) 199-208.

[10] M.R. de Brimont, C. Dupont, A. Daudin, C. Geantet, P. Paybaud, J. Catal. 286 (2012) 153-164.

[11] P.T. Do, M. Chiappero, L.L. Lobban, D.E. Resasco, Catal. Lett. 130 (2009) 9-18.

[12] S. Lestari, I. Simakova, A. Tokarev, P. Maki-Arvela, K. Eranen, D.Y. Murzin, Catal. Lett. 122 (2008) 247-251.

[13] Y. Bie, A. Gutierrez, T.R. Viljava, J.M. Kanervo, J. Lehtonen, Ind. Eng. Chem. Res. 52 (2013) 11544-11551.

[14] C. Ochoa-Hernández, Y. Yang, P. Pizarro, V.A. de la Peña O'Shea, J.M. Coronado,

D.P. Serrano, Catal. Today 210 (2013) 81-88.

[15] Q. Liu, Y. Bie, S. Qiu, Q. Zhang, J. Sainio, T. Wang, L. Ma, J. Lehtonen, Appl. Catal. B: Environ. 147 (2014) 236-245.

[16] C. Wang, Q. Liu, J. Song, W. Li, P. Li, R. Xu, H. Ma, Z. Tian, Catal. Today 234 (2014) 153-160.

[17] S. Bezergianni, S. Voutetakis, A. Kalogianni, Ind. Eng. Chem. Res. 48 (2009) 8402-8406.

[18] H. Zuo, Q. Liu, T. Wang, L. Ma, Q. Zhang, Q. Zhang, Energy Fuels 26 (2012) 3747-3755.

[19] Q. Liu, T. Wang, L. Ma, Q. Zhang, Appl. Catal. A: Gen. 468 (2013) 68-74.

[20] Y. Yang, C. Ochoa-Hernández, V.A. de la Peña O'Shea, J.M. Coronado, D.P. Serrano, ACS Catal. 2 (2012) 592-598.

[21] J. Duan, J. Han, H. Sun, P. Chen, H. Lou, X. Zheng, Catal. Commun. 17 (2012) 76-80.

[22] C. Ochoa-Hernández, Y. Yang, P. Pizarro, V.A. de la Peña O'Shea, J.M. Coronado, D.P. Serrano, Catal. Today 210 (2013) 81-88.

[23] A. Shrotri, L.K. Lambert, A. Tanksale, J. Beltramini, Green Chem. 15 (2013) 2761-2768.

[24] B. Ma, C. Zhao, Green Chem. 17 (2015) 1692-1701.

[25] B. Peng, Y. Yao, C. Zhao, J.A. Lercher, Angew. Chem. Int. Ed. 51 (2012) 2072-2075.

[26] K. Murata, Y. Liu, M. Inaba, I. Takahara, Energy Fuels 24 (2010) 2404-2409.

[27] B. Peng, C. Zhao, S. Kasakov, S. Foraita, J.A. Lercher, Chem. Eur. J. 19 (2013) 4732-4741.

[28] S.W. King, US Patent 5,191,123, 1993.

[29] S.W. King, US Patent 5,245,032, 1993.

[30] M.V. Ganduglia-Pirovano, A. Hofmann, J. Sauer, Surf. Sci. Rep. 62 (2007) 219-270.

[31] H. Hattori, Chem. Rev. 95 (1995) 537-558.

[32] G. Li, F. Zhang, L. Chen, C. Zhang, H. Huang, X. Li, ChemCatChem 7 (2015) 2646-2653.

[33] G. Leofanti, M. Padovan, G. Tozzola, B. Venturelli, Catal. Today 41 (1998) 207-219.

[34] W. Song, C. Zhao, J.A. Lercher, Chem. Eur. J. 19 (2013) 9833-9842.

[35] Q. Liu, F. Gu, X. Lu, Y. Liu, H. Li, Z. Zhong, G. Xu, F. Su, Appl. Catal. A: Gen. 488 (2014) 37-47.

[36] K.V. Manukyan, A.J. Cross, A.V. Yeghishyan, S. Rouvimov, J.J. Miller, A.S. Mukasyan, E.E. Wolf, Appl. Catal. A: Gen. 508 (2015) 37-44.

[37] Y. Bang, S. Park, S.J. Han, J. Yoo, J.H. Song, J.H. Choi, K.H. Kang, I.K. Song, Appl. Catal. B: Environ. 180 (2016) 179-188.

Figure captions

Figure 1. XRD patterns of Zn-Al composite precursors with different Zn/Al ratios: (a) 1/3, (b) 1/2, (c) 1/1, (d) 2/1 (e) 3/1, (f) 5/1.

Figure 2. XRD patterns of ZnO-Al_2O_3 supports with different Zn/Al ratios: (a) 1/3, (b) 1/2, (c) 1/1, (d) 2/1 (e) 3/1, (f) 5/1.

Figure 3. SEM images of ZnO-Al_2O_3 supports with different Zn/Al ratios: (a) 1/3, (b) 1/2, (c) 1/1, (d) 2/1 (e) 3/1, (f) 5/1.

Figure 4. TEM images of the reduced Ni-based catalysts with different Zn/Al ratios and their histograms of Ni species size distribution (inset): (a) 1/3, (b) 1/2, (c) 1/1, (d) 2/1 (e) 3/1, (f) 5/1.

Figure 5. H_2-TPR profiles of unreduced Ni-based catalysts with different Zn/Al ratios: (a) 1/3, (b) 1/2, (c) 1/1, (d) 2/1 (e) 3/1, (f) 5/1.

Figure 6. XRD patterns of the Ni-based catalysts with different Zn/Al ratios: (a) 1/3, (b) 1/2, (c) 1/1, (d) 2/1 (e) 3/1, (f) 5/1.

Figure 7. Ni 2p XPS spectra (A) and surface metallic Ni concentrations (B) of the catalysts with different Zn/Al ratios.

Figure 8. IR spectra of the liquid products obtained from different catalysts: (a) Ni/Zn1Al3, (b) Ni/Zn1Al2, (c) Ni/Zn1Al1, (d) Ni/Zn2Al1, (e) Ni/Zn3Al1, (f) Ni/Zn5Al1. Reaction conditions: oleic acid (2.0 g), decalin (30.0 g), catalyst (0.2 g), temperature (280 °C), H_2 pressure (2.5 MPa), and stirring at 600 r/min for 6 h.

Figure 9. Conversion of stearyl stearate over different catalysts versus reaction time: (a) Ni/Zn1Al3, (b) Ni/Zn1Al2, (c) Ni/Zn1Al1, (d) Ni/Zn2Al1, (e) Ni/Zn3Al1, (f)

Ni/Zn5Al1. Reaction conditions: stearyl stearate (2.0 g), decalin (30.0 g), catalyst (0.05 g), temperature (280 °C), H_2 pressure (2.5 MPa), and stirring at 600 r/min.

Table 1. Textural properties and Ni content of the Ni-based catalysts with different Zn/Al ratios.

Sample	Specific surface area (m^2/g)	Pore volume (cm^3/g)	Average pore size (nm)	Ni content (wt.%)
Ni/Zn1Al3	182	0.17	3.7	9.8
Ni/Zn1Al2	152	0.19	5.0	9.8
Ni/Zn1Al1	115	0.16	5.6	9.9
Ni/Zn2Al1	71	0.14	7.8	10.1
Ni/Zn3Al1	66	0.18	11.2	10.3
Ni/Zn5Al1	53	0.15	11.2	10.2

Table 2. HDO of oleic acid over the Ni-based catalysts with different Zn/Al ratios.

Catalyst	Conversion[a] (%)	Yields of liquid products (wt.%) [b]					
		n-C_{17}	*n*-C_{18}	1-octadecanol	Stearic acid	Stearyl stearate	Stearate
Ni/Zn1Al3	100	38.3	2.7	2.4	21.9	34.7	-
Ni/Zn1Al2	100	50.2	3.1	2.1	13.7	30.9	-
Ni/Zn1Al1	100	71.1	2.3	1.3	-	25.3	-
Ni/Zn2Al1	100	93.7	2.1	1.3	-	-	2.9
Ni/Zn3Al1	100	85.7	2.0	-	-	-	13.2
Ni/Zn5Al1	100	75.9	2.2	-	-	-	21.9

[a] This value represents the hydrogenation of double bond in the oleic acid.

[b] Reaction conditions: oleic acid (2.0 g), decalin (30.0 g), catalyst (0.2 g), temperature (280 °C), H_2 pressure (2.5 MPa), and stirring at 600 r/min for 6 h.

Table 3. HDO of stearyl stearate over the Ni-based catalysts with different Zn/Al ratios.

Catalyst	Selectivities of liquid products (wt.%) [a]			k (h^{-1}) [b]	R^2 [c]
	n-C_{17}	n-C_{18}	octadecanal		
Ni/Zn1Al3	80.3	19.7	0	0.048	0.998
Ni/Zn1Al2	84.9	15.1	0	0.074	0.998
Ni/Zn1Al1	82.0	14.4	3.6	0.086	0.997
Ni/Zn2Al1	76.1	13.2	10.7	0.095	0.997
Ni/Zn3Al1	52.8	14.1	33.1	0.066	0.996
Ni/Zn5Al1	37.1	12.3	50.6	0.056	0.998

[a] Reaction conditions: stearyl stearate (2.0 g), decalin (30.0 g), catalyst (0.05 g), temperature (280 °C), H_2 pressure (2.5 MPa), and stirring at 600 r/min for 6 h.

[b] Reaction rate constants of stearyl stearate were calculated by the pseudo-first-order kinetic equation.

[c] Correlation coefficient

Figure 1

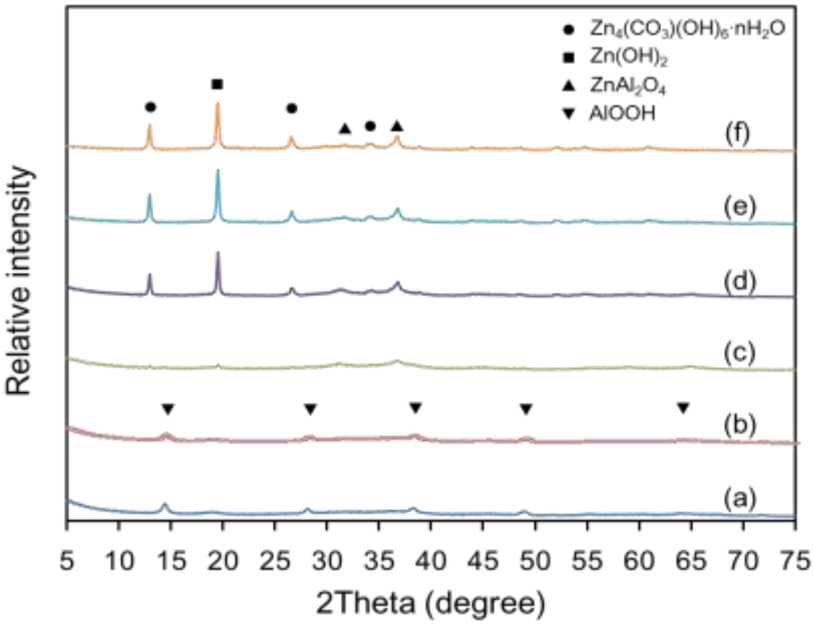
● $Zn_4(CO_3)(OH)_6 \cdot nH_2O$
■ $Zn(OH)_2$
▲ $ZnAl_2O_4$
▼ AlOOH
(f)
(e)
(d)
(c)
(b)
(a)
Relative intensity
5
10
15
20
25
30
35
40
45
50
55
60
65
70
75
2Theta (degree)

Figure 2

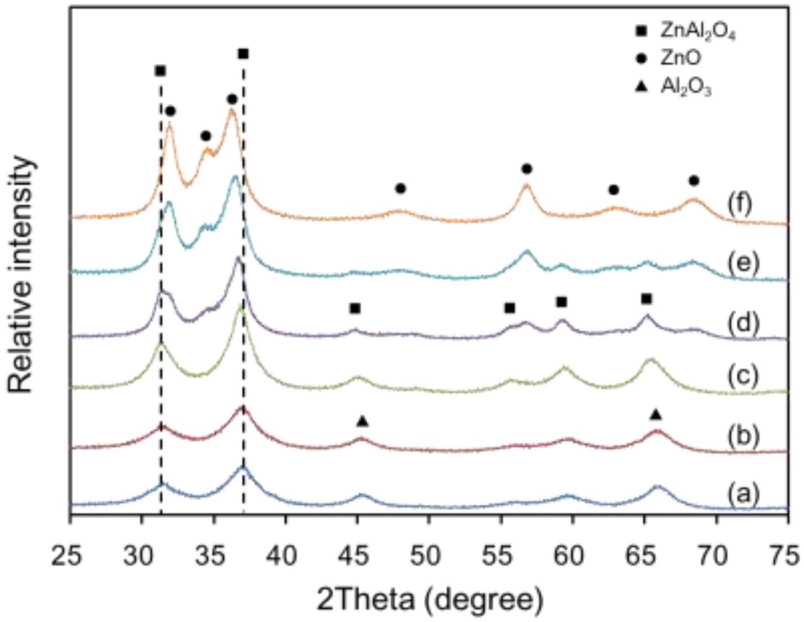
■ $ZnAl_2O_4$
● ZnO
▲ Al_2O_3
Relative intensity
2Theta (degree)
25
30
35
40
45
50
55
60
65
70
75
(f)
(e)
(d)
(c)
(b)
(a)

Figure 3

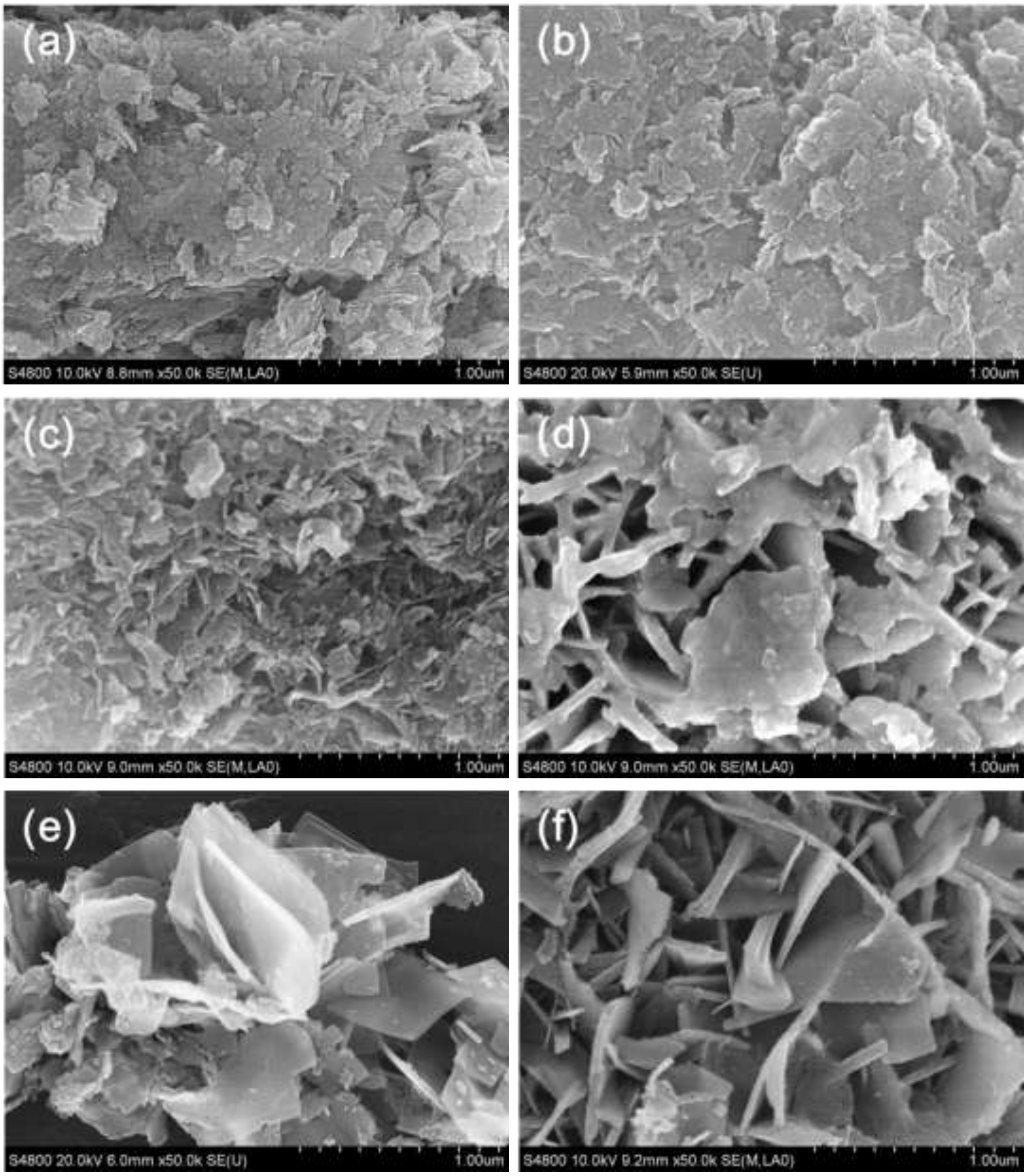
(a)
S4800 10.0kV 8.8mm x50.0k SE(M,LA0)
1.00um
(b)
S4800 20.0kV 5.9mm x50.0k SE(U)
1.00um
(c)
S4800 10.0kV 9.0mm x50.0k SE(M,LA0)
1.00um
(d)
S4800 10.0kV 9.0mm x50.0k SE(M,LA0)
1.00um
(e)
S4800 20.0kV 6.0mm x50.0k SE(U)
1.00um
(f)
S4800 10.0kV 9.2mm x50.0k SE(M,LA0)
1.00um

Figure 4

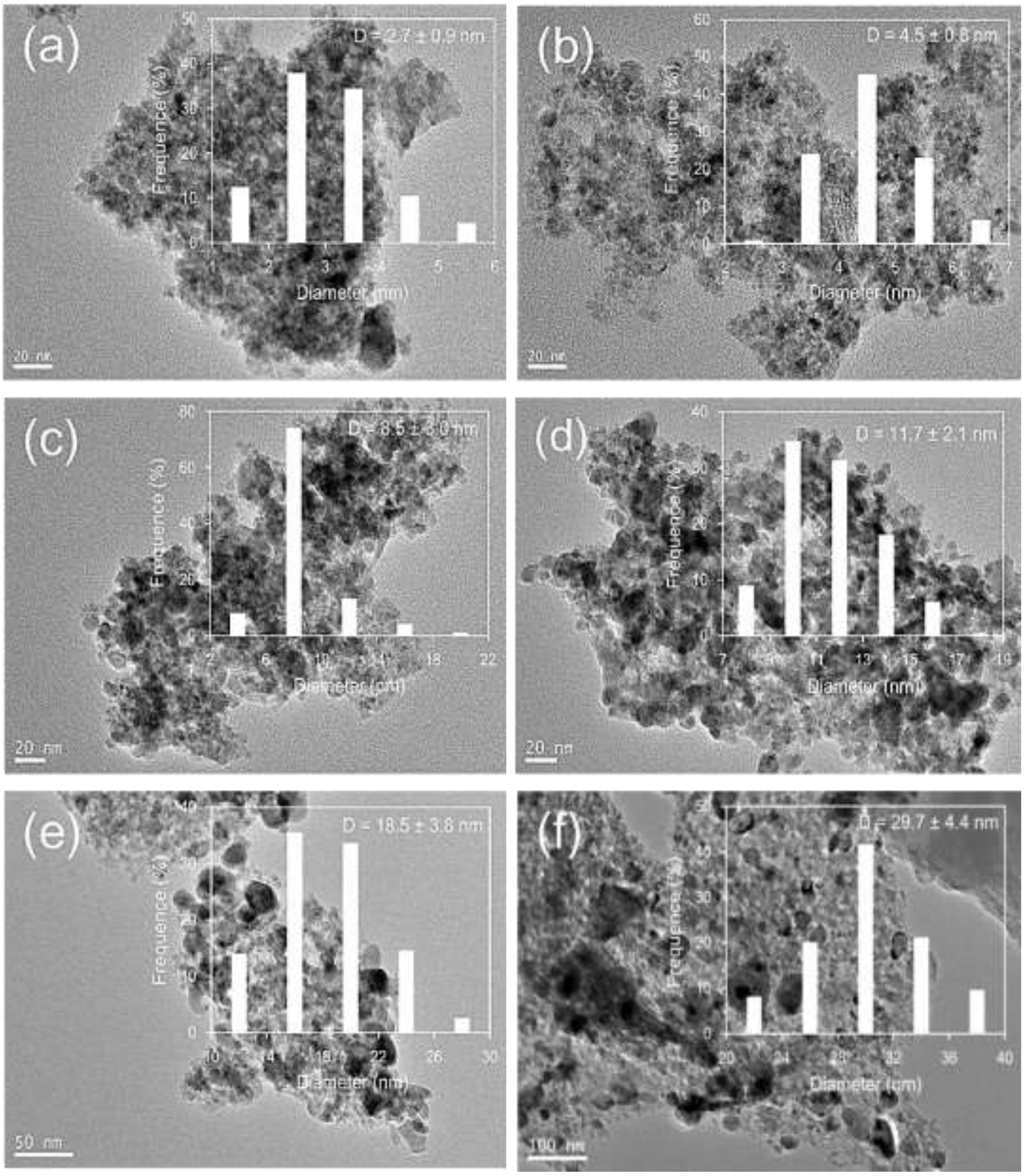
(a)
D = 2.7 ± 0.9 nm
Frequence (%)
Diameter (nm)
20 nm
(b)
D = 4.5 ± 0.8 nm
Frequence (%)
Diameter (nm)
20 nm
(c)
D = 8.5 ± 3.0 nm
Frequence (%)
Diameter (nm)
20 nm
(d)
D = 11.7 ± 2.1 nm
Frequence (%)
Diameter (nm)
20 nm
(e)
D = 18.5 ± 3.8 nm
Frequence (%)
Diameter (nm)
50 nm
(f)
D = 29.7 ± 4.4 nm
Frequence (%)
Diameter (nm)
100 nm

Figure 5

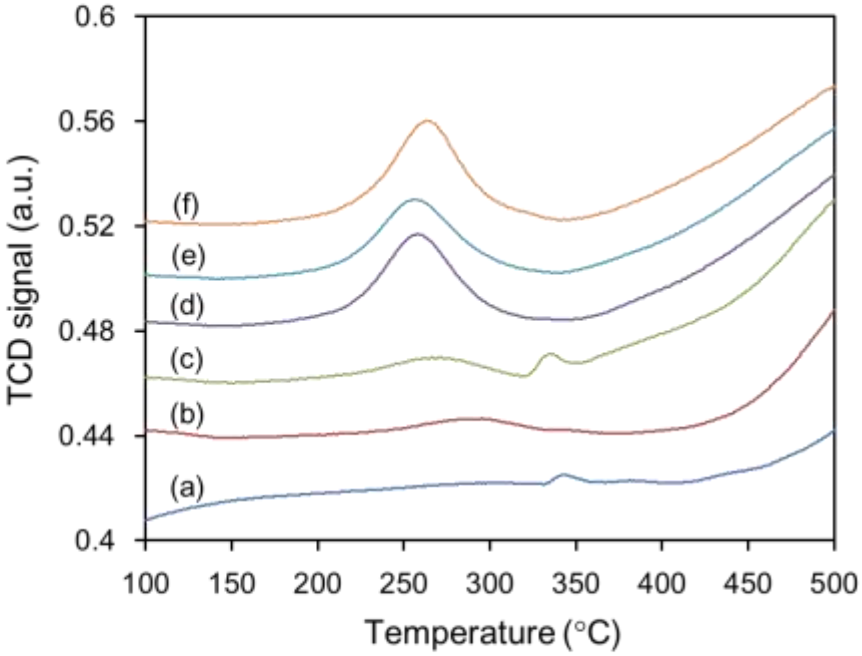
0.6
0.56
0.52
0.48
0.44
0.4
TCD signal (a.u.)
(f)
(e)
(d)
(c)
(b)
(a)
100
150
200
250
300
350
400
450
500
Temperature (°C)

Figure 6

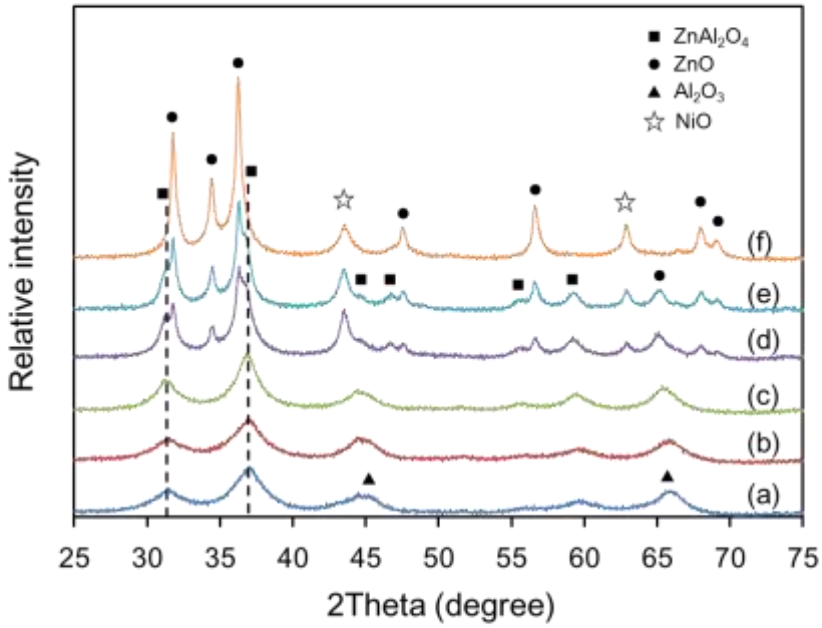
■ ZnAl2O4
● ZnO
▲ Al2O3
☆ NiO
Relative intensity
2Theta (degree)
(a)
(b)
(c)
(d)
(e)
(f)
25
30
35
40
45
50
55
60
65
70
75

Figure 7

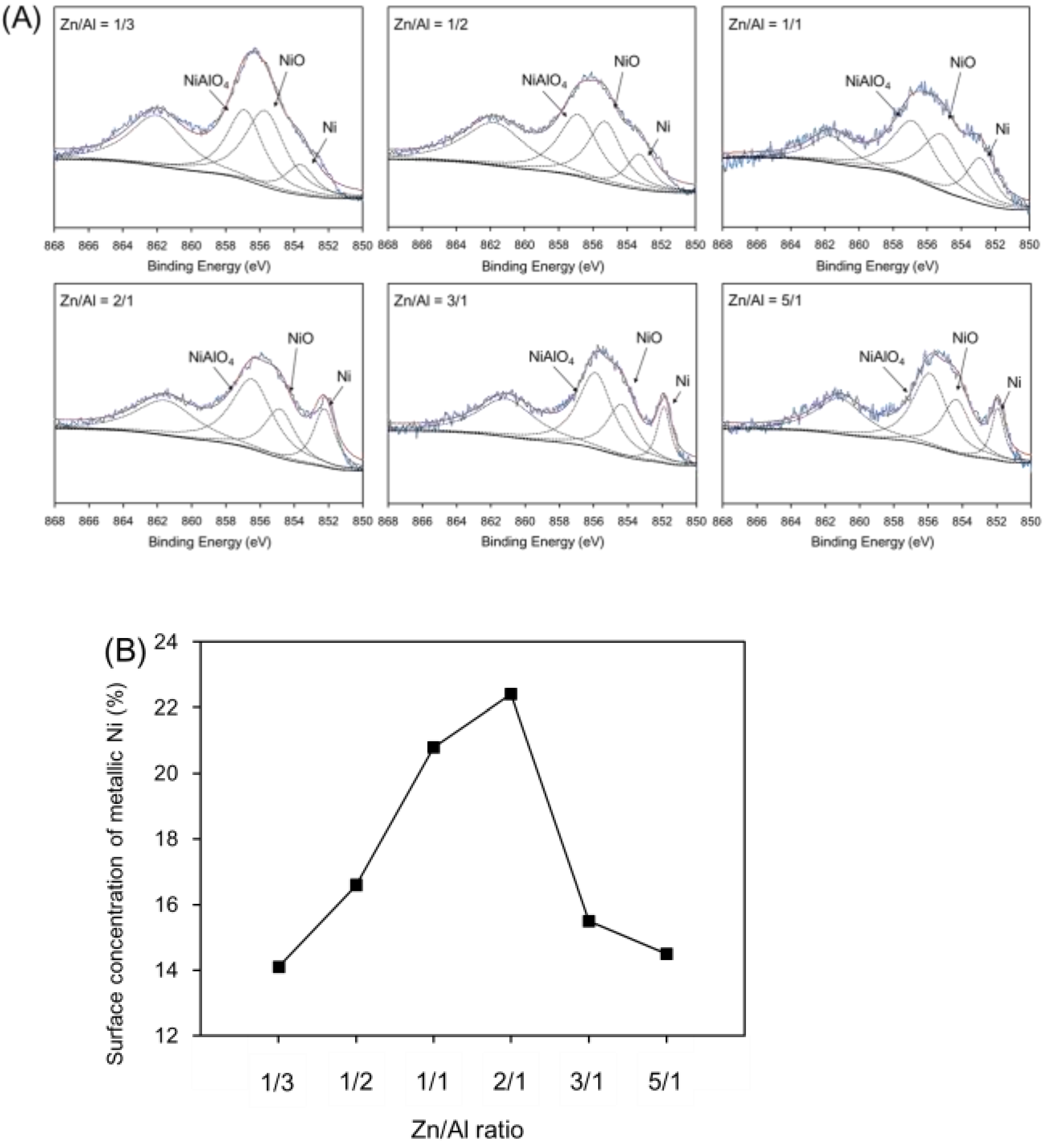
(A)
Zn/Al = 1/3
Zn/Al = 1/2
Zn/Al = 1/1
Zn/Al = 2/1
Zn/Al = 3/1
Zn/Al = 5/1
NiAlO$_4$
NiO
Ni
868 866 864 862 860 858 856 854 852 850
Binding Energy (eV)
(B)
Surface concentration of metallic Ni (%)
24 22 20 18 16 14 12
1/3 1/2 1/1 2/1 3/1 5/1
Zn/Al ratio

Figure 8

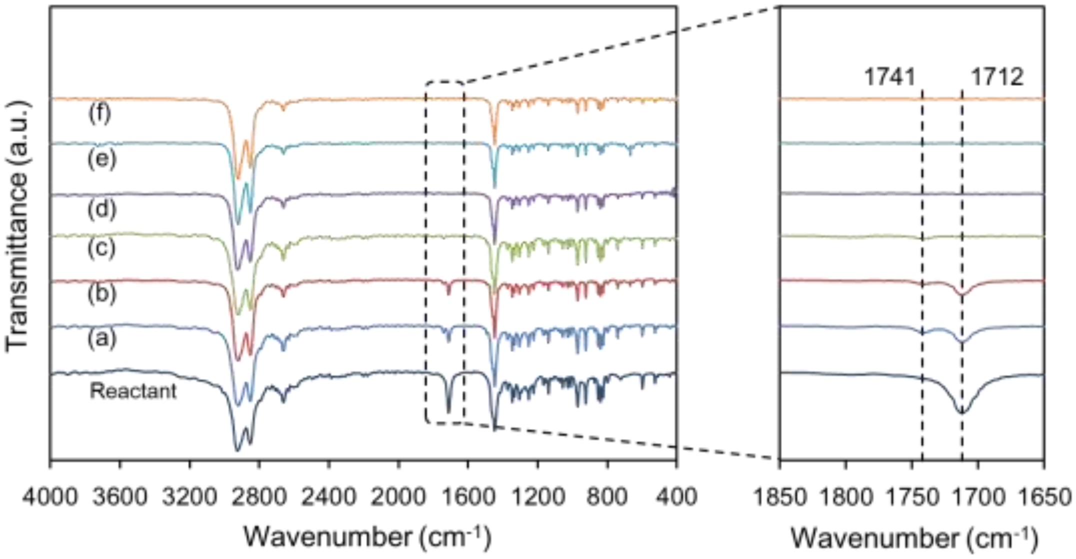
Transmittance (a.u.)
(f)
(e)
(d)
(c)
(b)
(a)
Reactant
4000
3600
3200
2800
2400
2000
1600
1200
800
400
Wavenumber (cm-1)
1741
1712
1850
1800
1750
1700
1650
Wavenumber (cm-1)

Figure 9

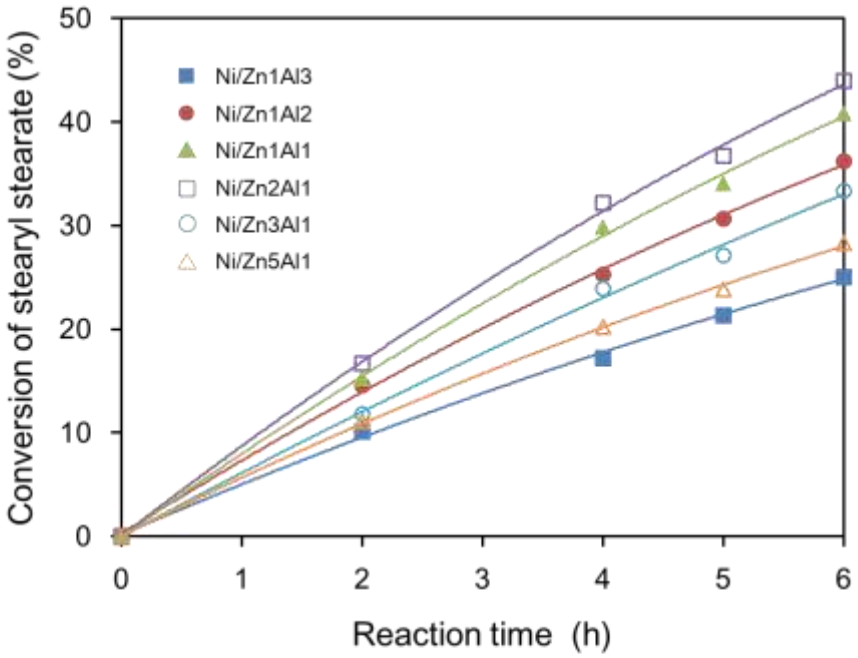
Ni/Zn1Al3
Ni/Zn1Al2
Ni/Zn1Al1
Ni/Zn2Al1
Ni/Zn3Al1
Ni/Zn5Al1
Conversion of stearyl stearate (%)
0
10
20
30
40
50
0
1
2
3
4
5
6
Reaction time (h)